EXPERIMENTAL CHARACTERIZATION OF A MAGNETOHYDRODYNAMIC PLASMA ACTUATOR FOR STALL ALLEVIATION

Young-Joon Choi
Undergraduate Research Assistant,

Jayant Sirohi
Assistant Professor
jayant.sirohi@mail.utexas.edu,

Laxminarayan Raja
Professor

Department of Aerospace Engineering and Engineering Mechanics
The University of Texas at Austin,
Austin, TX 78712, United States

OVERVIEW

An experimental investigation of a magnetohydrodynamic plasma actuator, called Rail Plasma Actuator (RailPAc), was conducted to evaluate its potential for aerodynamic flow control. The actuator consisted of a pair of parallel rails, each with a length of 0.25 *m* and separated by 0.01 m air gap, embedded chord-wise on the surface of S5010 airfoil section with a span of 0.82 *m* and a chord of 0.37 *m*. A custom built trigger circuit initiated a Townsend avalanche through a volume of air between the rails and the resulting plasma armature was propelled downstream by self-induced electromagnetic fields created by a low-voltage and high current discharge. This motion of the plasma armature transferred momentum to the surrounding air and induced flow on the surface of the airfoil. High-speed imaging, electrical measurements, and force measurements were performed to quantify the characteristics of the RailPAc. It was observed that the plasma armature reached peak velocity of 60 *m/s* with 1.2 *kA* peak current discharge. A transient reaction force with a peak of 8 *N* from RailPAc was exerted on the airfoil.

NOMENCLATURE

AC	=	Alternating current
C	=	Capacitance
DBD	=	Dielectric barrier discharge
DC	=	Direct current
EHD	=	Electrohydrodynamic
F	=	Forcing function
G	=	Impulse response transfer function
I	=	Current
L	=	Inductance
MHD	=	Magnetohydrodynamic
R	=	Resistance
T	=	Period
t	=	Time domain
q	=	Charge
s	=	Frequency domain
u_0	=	Permeability of Free Space
X	=	Structural response function
ω_n	=	Natural frequency

1. INTRODUCTION

The lift and drag characteristics of an airfoil are a function of its angle of attack and the incoming free stream velocity. The development of flow separation at high angles of attack causes an airfoil to stall and the mechanisms that delay this onset of separation are a subject of active research. In a helicopter, the rotation of the blades causes a variation in free stream velocity and angle of attack once per rotation. Hence, a helicopter at a high forward flight speed can periodically experience dynamic stall on the retreating side of the rotor disk, limiting its maximum flight speed.

Methods to address the problem of dynamic stall include the use of passive devices, such as leading edge slats [1], air injection [2], and suction [3] that operate continuously, and active devices that periodically energize the boundary layer when the blade is at the retreating side. On the other hand, actuators based on electro-

hydrodynamics or magnetohydrodynamics provide less mechanically complex methods to alleviate stall by energizing the boundary layer without moving parts [4].

Two types of plasma actuators, electro-hydrodynamic (EHD) and magneto-hydrodynamic (MHD), are subject of active research. The most common type of EHD actuator, the Dielectric Barrier Discharge (DBD) actuator, consists of two electrodes, one exposed to air and flush mounted on the surface of the airfoil and the other embedded within the dielectric airfoil. High voltage, on the order of tens of *kV*, is applied between the two electrodes to create a sheath of plasma. This resulting ionized region, in the presence of electric field, creates a body force that entrains the flow near the electrodes [5]. Previous works on DBD have shown that this type of plasma actuator can be used for boundary layer separation control for turbine blades [6] and dynamic stall vortex control [7]. However, the effectiveness of these actuators has not been demonstrated at high Reynolds numbers and Mach numbers representative of full-scale flight vehicles.

MHD plasma actuators utilize electromagnetic fields to accelerate a region of plasma using the Lorentz force. The electrodes are flush mounted on the airfoil surface and exposed in air. When a plasma arc forms across the electrodes, the interaction between the current through the plasma and the magnetic field gives rise to a body force that moves the plasma. Previous study conducted by Zaidi et al. [8] has shown that the MHD concept could be applied to high-speed boundary layer control. Their concept, known also as the “snowplow” actuator, utilized a permanent magnet to provide the necessary magnetic field.

A novel MHD actuator presented in this paper, the Rail Plasma Actuator, or RailPAc, uses a self-induced magnetic field for plasma motion. Studies by Pafford et. al. [10], have shown that RailPAc is capable of achieving a peak arc velocity of 100 *m/s* and can induce flow around 20 *m/s*. The objective of this paper is to expand upon his studies by determining the velocity and electrical characteristics of the RailPAc system mounted on the S5010 airfoil section and examine the body force exerted on the airfoil in a static environment.

2. PRINCIPLE OF OPERATION

In the case of a conventional electromagnetic rail gun, the current loop formed by the rails and the conductive armature induces a magnetic field. The resulting Lorentz force accelerates the plasma armature in the direction perpendicular to both the current and the magnetic field.

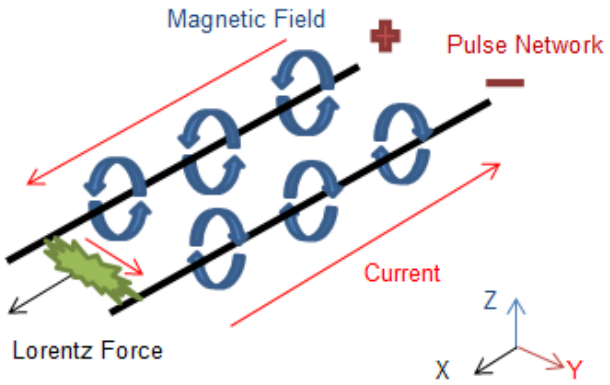

Figure 1: Schematic of the RailPAc system.

The RailPAc applies this concept to flow control with a plasma armature, rather than with a solid armature. When a large potential difference is applied across the air gap between the rails, a DC electric breakdown of air, known as a Townsend avalanche, occurs. The formation of this packet of weakly ionized plasma, or plasma armature, creates a localized high conductivity region that permits high current flow across the air gap between the rails. As shown in figure 1, the current generated by the pulse network induces a net magnetic field in the positive Z-direction between the rails. The plasma armature conducts the current flow in the positive Y-direction. The Lorentz force, which is the cross product of the current and the magnetic field, accelerates the plasma armature in the positive X-direction and drives the armature in a manner similar to that of an electromagnetic rail gun [10].

If operated in quiescent air, the RailPAc can induce transient flow through the body force imparted by the moving plasma armature and the thermal expansion produced by joule heating of the plasma. It is the momentum transfer initiated by the moving plasma armature that is of interest for flow control [8].

The plasma armature can be modeled as a solid body [9] that causes a region of compression in front and entrainment behind its transit. This pressure gradient can accelerate the otherwise quiescent air and thus have a potential application in boundary layer separation control.

The RailPAc can be embedded conformal to the airfoil profile, requires no moving parts, and has a negligible weight penalty [10]. Such characteristics make the RailPAc quite suitable for highly vibratory and weight sensitive environment experienced on helicopter blades. In the future, the RailPAc could be initiated once per revolution on the retreating side of the blade, increasing the maximum lift as well as the forward flight speed of the helicopter. In case of an actuator failure, the airfoil would simply revert to its passive state without any aerodynamic penalty.

3. EXPERIMENTAL SETUP

Tests were performed on a S5010 airfoil with a span of 0.82 *m* and a chord of 0.37 *m*. The RailPAc actuator consisted of two parallel copper rails, each with a length of 0.25 *m*, width of 0.01 *m*, and 0.01 *m* separation gap, mounted conformally to the upper surface of the airfoil along the chord-wise direction. In all cases, the RailPAc was operated in quiescent air.

The arc initiation point was at 10% of chord and the rail ended at 80% of chord. Figure 2 is a picture of the test article.

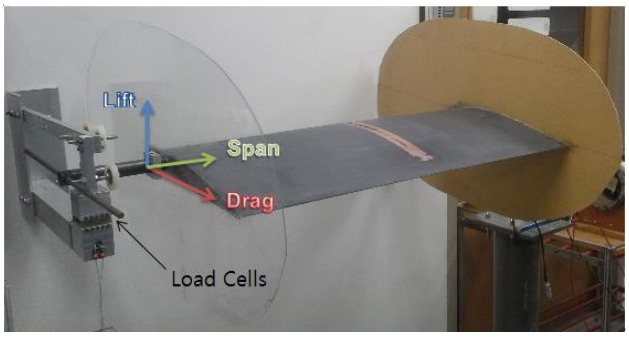

Figure 2: S5010 Test Article with embedded RailPAc system as viewed from the trailing edge. Load cells are mounted on both sides of the airfoil.

The plasma arc was initiated by a trigger circuit consisting of a variable transformer and an AC-DC converter. The circuit provided a step-up voltage transformation from main line to around 35 *kV* DC discharge required for the Townsend avalanche. To ensure consistency in the discharge location, small copper pieces were added to each rail at the leading edge for a localized decrease in air gap distance between the rails.

The current to drive the plasma armature was supplied by a pulse network. Schematic is shown in figure 3.

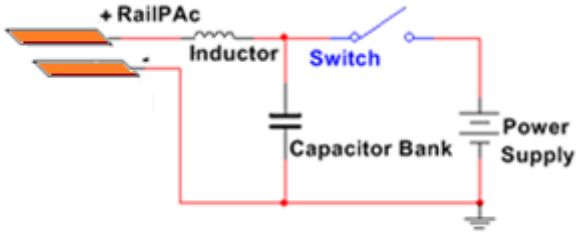

Figure 3: Circuit Diagram of Pulse Network

A Xantrex XHR 600-1.7 DC power supply was used to charge the 21 *mF* capacitor bank comprised of six parallel electrolytic capacitors to 250 *V*. The capacitor bank was discharged through a 110 *μH* air coil inductor connected in series with the rails. Once the trigger circuit initiated a plasma arc across the rails, a pulsed discharge on the order of *kA* occurred.

The schematic shown in figure 3 can be modeled as a second order RLC circuit, with governing differential equation in terms of charge q(t) given by equation (1):

(1) $$\frac{d^2q(t)}{dt^2} + \frac{R}{L}\frac{dq(t)}{dt} + \frac{1}{LC}q(t) = 0$$

This second order equation is characterized by the natural frequency, ω_n:

(2) $$\omega_n = \sqrt{\frac{1}{LC}}$$

The period of oscillation for the undamped second order system is given by:

(3) $$\mathrm{T} = 2\pi\sqrt{LC}$$

Note that in the case of the RailPAc, the resistance R is the sum of plasma resistance and electrical component resistance. While plasma resistance is an unkown function of time,

the component resistance was measured to be 0.11 Ω based only on the inductor wiring and capacitor bank resistance. Predicted current pulse with the nominal component values is shown in figure 4.

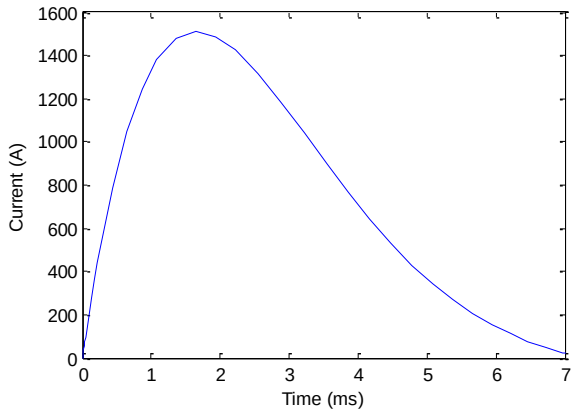

Figure 4: Simulated theoretical response of RailPAc pulse current with constant resistance assumption.

An estimate of T=7 *ms* can be obtained solving equation (1) with the given component values. A peak current of 1.5 *kA* is predicted by the model.

3.1. Velocity Measurements

Vision Research Phantom v5.1 high speed camera was used to obtain the velocity profile of the plasma armature. The resolution was set to 256×256 pixels with frame rate of 13029 frames per second. The exposure time was limited to 72 *μs*. A mylar film was mounted in front of the camera lens as a filter. The distance scale factor was set to 1 *mm/pixel*. The camera was mounted normal to the airfoil and centered at the rails.

3.2. Electrical Measurements

Data acquisition of the electrical measurements was performed using the National Instrument cDAQ 9172 with voltage range of ±10 *V* at a sampling rate of 36 *kHz*.

A Pearson 110A current transformer and a custom made Rogowski coil were used to measure the RailPAc pulse current. The Pearson probe was manufacturer calibrated to 0.1 *A/V*. Because the calibration factor for the Rogowski coil was unknown, measurements from the Rogowski coil and the Pearson probe were correlated at low currents to find the current-voltage conversion factor for the Rogowski coil.

3.3. Force Measurements

Force measurements were conducted with load cells to measure lift components of the net force exerted on the airfoil. The steel spar of the airfoil was clamped on each side to L-brackets system, thus providing a rigid support platform for the airfoil. The load cells used were Omega LCL-005. The load cells were mounted on 0.20 *mm* thick bronze plates to add stiffness and minimize off-axis sensitivity. The load cells were oriented such that positive voltage output corresponded to negative lift direction.

The outputs of the load cells were amplified with RaeTech strain gage amplifiers at a gain of 200. The outputs of the amplifier were subjected to a first order anti-aliasing filter with a cutoff frequency at 1.2 *kHz*. The data acquisition was performed at a sampling frequency of 9 *kHz*. The linearity of the load cells was verified using measurement of the static force-displacement characteristics.

3.3.1. Impulse Hammer Test

In case of a steady state actuation, the constant forcing applied to the airfoil permits the direct conversion of the load cell voltage into force measurement. However, the RailPAc exerts a transient force on the airfoil. In such case, a time history of the forcing function is needed, which can be obtained by deconvolving the load cell impulse response functions from the measured load cell response.

The impulse response function, which serves as the transfer function between the structural response and the applied forcing, was obtained using the impulse hammer test. Tektronix PCB-4461 impulse hammer was used to excite the airfoil in the lift direction. It was assumed that the chord-wise impact position would not yield any appreciable change in the structural response. However, the span-wise strike location was kept constant at the RailPAc position because a deviation could cause excitation in rolling mode of the airfoil, rather than in translational mode.

The forcing function in time domain was obtained with the piezoelectric force gauge

mounted in the hammer and the structural response was simultaneously obtained from the load cells. A common sampling rate of 9 *kHz* was used for both the load cells and the impulse hammer. The signal from the impulse hammer was amplified with a gain of 10 and the impulse hammer was calibrated to 2.23 *mV/N*.

4. RESULTS AND DISCUSSION

4.1. Velocity Measurements

The plasma armature was clearly visible moving along the rails as seen in figure 5, which shows frames from the high-speed video of the top view of the airfoil with orange rectangles indicating rail outline.

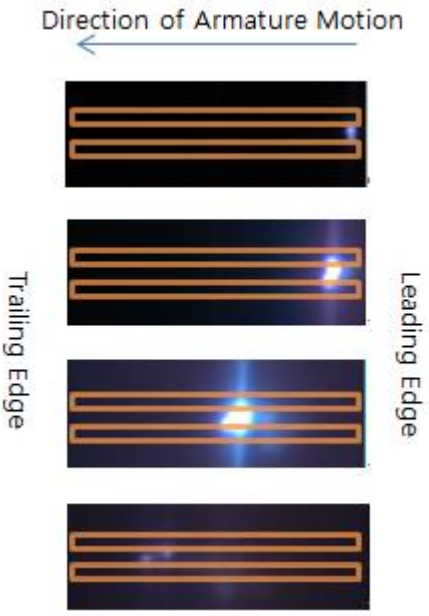

Figure 5: Progression of the plasma armature, from top to bottom, at 0.156 *ms*, 0.921 *ms*, 3.146 *ms*, 5.056 *ms* referenced from the initial formation of the armature.

An afterglow region could be seen trailing the plasma armature, especially at 3.146 *ms* and 5.056 *ms* after the armature formation. This indicated a strong region of electromagnetic field in the space occupied by the plasma armature, but an immediate weakening field after the transit. It was also observed that the plasma armature did not transit across the entire rail and was extinguished at 0.2 *m* downstream from the initiation point, which corresponded to 70% of chord location.

At some instances, two plasma armatures were seen instead of a single one. This is shown in figure 6.

Figure 6: Separation of plasma armature taken at 2.916 *ms* after the initial formation of the armature.

Rather than a smooth transit of a single clearly defined plasma armature, the armature stopped at certain regions of the rail and split into a larger armature and a smaller armature. This smaller armature continued to move down the rails, while the larger armature was immobile. When the smaller armature travelled some distance down the rail, the larger armature moved to the new location of the smaller armature. Because of the limitations in frame rate, it was not possible to determine whether the movement was continuous.

This splitting phenomenon was due to local asperities of the rail surface. Such irregularities would tend to create a more favorable region of plasma existence based on the changes in gap distance along the rails. Therefore, a strong region of plasma would form at the most favorable location, while a certain amount of plasma would continue to transit due to the strong Lorentz force exerted by the induced electromagnetic field. Once the weaker and smaller plasma armature reached the next favorable region, the strong plasma armature would jump and merge with the smaller plasma armature. The repeated observation of such occurrences at approximately the same location on the rails gave credence to this argument.

Split in plasma armature would be problematic for flow control, since sudden variation in strength of plasma would disrupt the mean flow of the surrounding medium. However, it was seen that the split occurred some duration after the initial discharge, when the current, hence the induced magnetic field, was weakened. Thus, in the initial part of the discharge, the effect of the Lorentz forcing dominated the behavior. An incident airstream would have similar impact in adding momentum and therefore the splitting phenomenon should be reduced.

The location of the plasma armature was

measured from the high-speed video and differentiated using a central difference method. Figure 7 shows the resultant velocity profile.

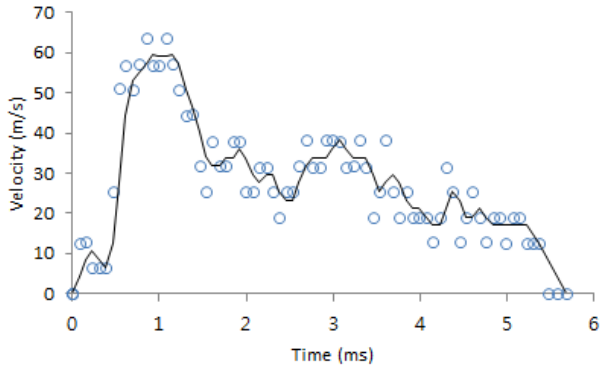

Figure 7: Flow velocity in time domain. Blue scatter plot represents velocity obtained from differentiation. Black line is three-point moving average to emphasize the mean velocity profile.

A peak velocity of 60 *m/s* was calculated around 1 *ms* after the plasma armature formation. Another velocity peak of 40 *m/s* was seen around 3 *ms*. It was concluded that plasma armature reached a terminal velocity in the initial part of its transit.

4.2. Electrical Measurements

A peak current of 1.2 *kA* during the pulsed discharge was measured using the Rogowski coil. Figure 8 plots the current as a function of time.

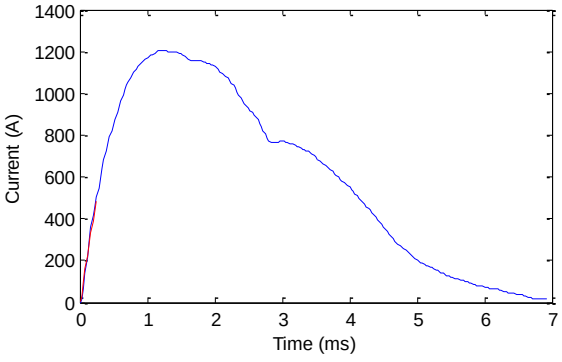

Figure 8: Measured current output from pulse network. Blue indicates measurement from the Rogowski coil, red is from the Pearson 110A current transformer.

Comparing figure 7 and figure 8, it can be seen that the peak velocity around 1 *ms* corresponded with the peak current output instance. It was also seen that the velocity peak around 3 *ms* corresponded with the small current increase seen at the same time. The deviation of the trend shown in figure 8 from that of an ideal overdamped RLC circuit response is the result of varying resistance in the plasma armature.

Induced magnetic field strength can be calculated with current, I, chord-wise armature location, j, and location between rails, r, using the Biot-Savart law:

(5) $$\mathrm{B(j,r)} = \frac{u_0}{4\pi}\int \frac{I\, dj \times r}{|r^3|}$$

For this analysis, the RailPAc rails were assumed to be two thin finite length wires separated by rail spacing, d = 0.01 m.

I and j were determined experimentally as a function of time from the current measurement and the high-speed camera. Since the magnetic field strength varies with r, an average magnetic field strength at some j can be determined.

(6) $$\bar{B}(j) = \frac{1}{d}\int_0^d B(j,r)dr$$

Using equation (6), the magnetic field strength as a function of time was determined and is shown in figure 9.

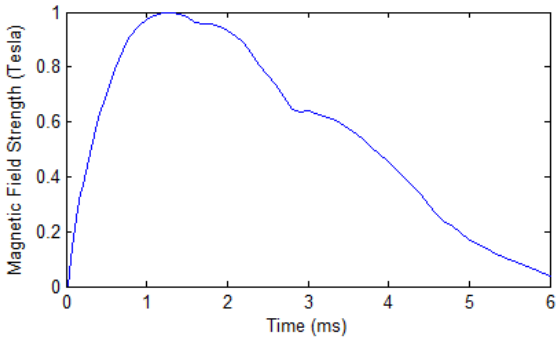

Figure 9: Induced magnetic field strength at the armature position.

The magnetic field strength had a similar profile to that of the current pulse, indicating that the armature position had negligible influence in the field strength. A peak magnetic field strength of 1 Tesla was seen at 1 ms.

4.3. Force Measurements

In order to obtain the impulse response transfer function, the fast Fourier transform was used to

transform the forcing function F(t), response function X(t), and the transfer function G(t) in time domain to the complex frequency domain. The convolution theorem in complex frequency domain states that the response is given by equation (7):

$$X(s) = G(s)F(s) \quad (7)$$

Therefore, the knowledge of X(s) and G(s), or correspondingly X(t) and G(t), is a necessary and sufficient condition to obtain F(s) and F(t).

With equation (7), the structural response obtained from the strain gages and the nature of the forcing obtained from the impulse hammer can be used to obtain a unique transfer function of the structure.

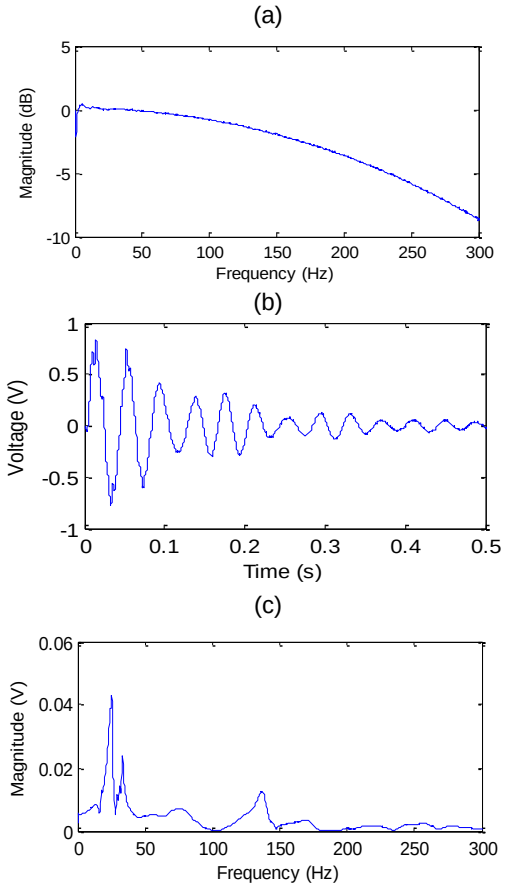

Figure 10: (a) Impulse hammer signal in frequency domain, (b) Lift load cell response in time domain and in (c) frequency domain.

As can be seen from figure 10a, the impulse hammer was able to excite the structure at a bandwidth of 200 *Hz*. The first mode of the structural response was detected at 26 *Hz*. The relatively low natural frequency of the structure in comparison to the wide bandwidth of the impulse hammer strike gave credence to the measured response of the structure, since the impulse hammer was able to excite the dominant modes of the structure.

The transfer function between load cell voltage and impulse hammer voltage was obtained and is graphed in figure 11.

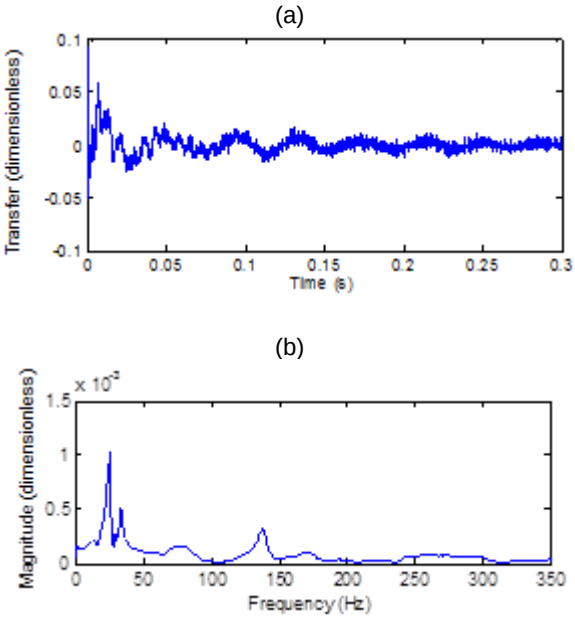

Figure 11: Lift transfer function in (a) time domain and (b) frequency domain.

Large high frequency noise was superimposed onto the transfer function due to the absence of anti-aliasing filter for the impulse hammer signal. Despite the noise, underlying impulse response function can clearly be identified, characterized by its logarithmic decrement and the dominance of the first modal frequency.

In order to verify the validity of the extracted transfer function, it was deconvoluted from structural response function to compare the resultant forcing function to that of the impulse hammer signal. To increase the clarity of the deconvoluted signal, an 8^{th} order Butterworth low pass filter was applied to the signals in both forward and reverse IIR filtration. This bidirectional filtration removes the phase distortion brought forth by the digital filtration delay and effectively doubles the filtration order. Figure 12 compares the actual force signal from the impulse hammer versus the forcing function obtained with deconvolution.

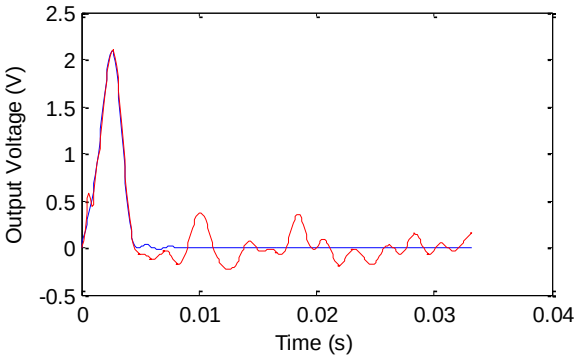

Figure 12: Comparison of actual forcing (shown in blue) and deconvoluted forcing (shown in red) in time domain.

In time domain, the deconvoluted forcing function matches the actual forcing function closely, albeit with some noise. This match validated the methodology and the same technique was applied to the RailPAc forcing.

The structural response from RailPAc forcing was obtained using the same setup was the impulse hammer test. In order to increase the signal to noise ratio, thirty structural responses from the RailPAc forcing was synchronously averaged. Figure 13 shows the resultant averaged response in time domain.

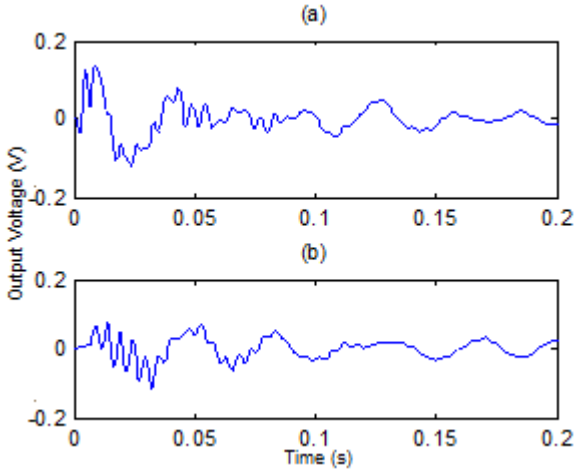

Figure 13: Synchronously averaged lift load cell response from (a) right end of airfoil, (b) left end of airfoil.

The transfer function was deconvoluted out of the response function in order to determine the nature of the RailPAc forcing function, using equation (7). The result for the lift force is shown in figure 14.

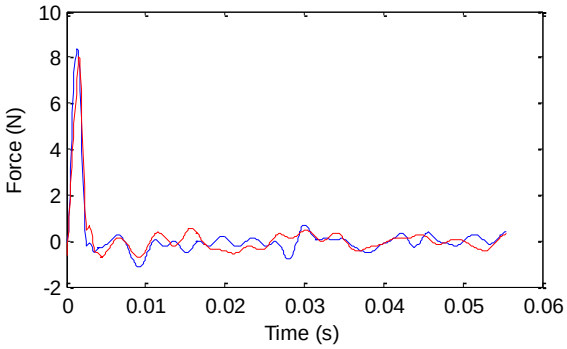

Figure 14: Deconvoluted lift forcing from left end of airfoil in blue and right end of airfoil in red.

The transfer function was deconvoluted out of the response function in order to determine the nature of the RailPAc forcing function, using equation (7). As shown in figure 14, the lift force extracted from load cells mounted in positive and negative span side of the airfoil correspond closely to each other. The peak of the response was detected at 8 *N* at 1 *ms* after the trigger circuit discharge. The forcing began immediately after the discharge and lasted for 2 *ms*.

The duration of the forcing suggested that the measured reaction was a direct result of the initial arc transit corresponding to the maximum current output. No aerodynamic force was detected, which would have occurred 20 *ms* after the arc transit based on the Laser Doppler Anemometry meausrements [10]. Thus, the force detected from the deconvolution was a reaction force from the plasma armature transit.

In comparsion, Thomas et al. [12] measured maximum thrust of 0.33 *N/m* with the DBD actuators in steady state operation. For the dimension of the RailPAc rails, DBD of comparable size would yield a thrust force of 0.083 *N*. It should be noted that the RailPAc force measurement was obtained in lift direction with a transient response, so a direct comparison with the DBD actuators cannot be made. However, one can roughly asses the order of magnitude difference in body force measurement between the two actuators.

In summary, a peak current pulse of 1.2 *kA* for 7 *ms* duration was detected, propelling the plasma armature to a peak velocity of 60 *m/s*. A peak force of 8 *N* was observed arising from the body force imparted by the plasma armature.

5. CONCLUSION

An experimental investigation of a magnetohydrodynamic plasma actuator was performed in the experiments presented in this paper. The setup consisted of a pair of rails 0.01 *m* by 0.25 *m* with separation distance of 0.01 m conformaly mounted on a S5010 airfoil with an attached pulse network and trigger circuit.

High-speed imaging was conducted to determine the velocity profile of the plasma armature. It was seen that a peak velocity of 60 *m/s* was achieved at 1 *ms* after the initial plasma armature formation. The electrical measurements showed that the pulse network provided a peak current of 1.2 *kA* for a pulse duration of 7 *ms*.

Force measurement was conducted using the load cells and deconvolution method to determine the lift applied to the airfoil by RailPAc. It was observed that the RailPAc pressed down on the airfoil with an 8 *N* impulsive force lasting for 2 *ms*.

Future work will include testing in the wind tunnel to determine the effect of RailPAc forcing in a moving air, rail geometry variation, actuation frequency and duty cycle analysis, and Particle Image Velocimetry (PIV) to gain a more indepth understanding of the RailPAc performance in boundary layer separation control.

6. REFERENCES

[1] Carr, L.W., and McAlister, K, "The Effect of a Leading Edge Slat on the Dynamic Stall of an oscillating Airfoil," *AIAA Paper 83-2533, AIAA/AFS Aircraft Design, Systems, and Operations Meeting*, Ft. Worth TX, Oct. 1983.

[2] Yu, Y.H., McAlister, K.W., Tung, C., and Wang, C.M., "Dynamic Stall Control for Advanced Rotorcraft Application," *AIAA Journal, Vol.33, No. 2*, Feb. 1995, pp. 289-295.

[3] Karim, M.A. and Achyara, M., "Control of the Dynamic Stall Vortex over a Pitching Airfoil by Leading Edge Suction," *AIAA Paper 93-3267, Shear Flow Conference*, Orlando FL, Jul. 1993.

[4] Artana, G., and Adamo, J. D., "*Flow Control with Electrohydrodynamic Actuators*", AIAA Paper 2001-0351, Aerospace Sciences Meeting & Exhibit, Reno, Nevada, Jan. 2001.

[5] Suzen, Y. B., and Huang, P. G., "Simulations of Flow Separation Control Using Plasma Actuators." AIAA Paper 2006-877, *Aerospace Sciences Meeting and Exhibit*, Reno, NV, Jan. 2006.

[6] Huang, J, Corke, T. C., and Thomas, F. O., "Plasma Actuators for Separation Control of Low-Pressure Turbine Blades", *AIAA Journal*, Vol. 44, No. 1, 2006, pp. 51-57.

[7] Post, M. L., and Corke, T. C., "Seperation Control Using Plasma Actuators-Dynamic Stall Vortex Control on an Oscillating Airfoil," *AIAA Journal*, Vol. 44, No. 12, 2006, pp. 3125-3135.

[8] Zaidi, S. H., Smith T., Macheret S., Miles R. B.,"Snowplow Surface Discharge in Magnetic Field for High Speed Boundary Layer Control", AIAA Paper 2006-1006, *44th Aerospace Science Meeting and Exhibit*, Reno, Nevada, Jan. 2011.

[9] Kelkar, M., and Heberlein, J., "Physics of an Arc in Cross Flow," *Journal of Applied Physics*, Vol. 33, 2000, pp. 2172-2182.

[10] Pafford, B., Choi, Y., Sirohi, J., Raja, L. L., "Experimental Characterization of the RailPAc Plasma Flow Actuator", Paper AIAA 2013-2885, 44th AIAA *Plasma Dynamics and Laser Conferece*, San Diego, CA, June, 2013.

[11] Pai, S. T., and Zhang, Q., "Introduction to High Power Pulse Technology," *Advanced Series in Electrical and Computer Engineering*, Vol. 10, 1995, pp. 272-274.

[12] Thomas, F. O., Corke, T. C., Iqbal, M., Kozlov, A., and Schatzman, D., "Optimization of Dielectric Barrier Discharge Plasma Actuators for Active Aerodynamic Flow Control", AIAA Journal, Vol. 47, No. 9, 2009, pp. 2169-2178.

COPYRIGHT STATEMENT